J. Fluid Mech. (2022), *vol*. 938, A31, doi:10.1017/jfm.2022.181

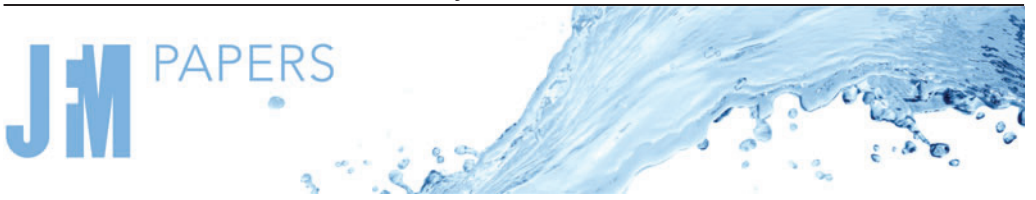

Heat transfer in turbulent Rayleigh–Bénard convection through two immiscible fluid layers

Hao-Ran Liu[1], **Kai Leong Chong**[2,†], **Rui Yang**[1], **Roberto Verzicco**[1,3,4] **and Detlef Lohse**[1,5,†]

[1]Physics of Fluids Group and Max Planck Center Twente for Complex Fluid Dynamics, MESA+ Institute and J. M. Burgers Centre for Fluid Dynamics, University of Twente, P.O. Box 217, 7500AE Enschede, The Netherlands

[2]Shanghai Key Laboratory of Mechanics in Energy Engineering, Shanghai Institute of Applied Mathematics and Mechanics, School of Mechanics and Engineering Science, Shanghai University, Shanghai 200072, PR China

[3]Dipartimento di Ingegneria Industriale, University of Rome 'Tor Vergata', Via del Politecnico 1, 00133 Roma, Italy

[4]Gran Sasso Science Institute – Viale F. Crispi 7, 67100 L'Aquila, Italy

[5]Max Planck Institute for Dynamics and Self-Organization, Am Fassberg 17, 37077 Göttingen, Germany

(Received 25 August 2021; revised 24 December 2021; accepted 25 February 2022)

We numerically investigate turbulent Rayleigh–Bénard convection through two immiscible fluid layers, aiming to understand how the layer thickness and fluid properties affect the heat transfer (characterized by the Nusselt number Nu) in two-layer systems. Both two- and three-dimensional simulations are performed at fixed global Rayleigh number $Ra = 10^8$, Prandtl number $Pr = 4.38$ and Weber number $We = 5$. We vary the relative thickness of the upper layer between $0.01 \leq \alpha \leq 0.99$ and the thermal conductivity coefficient ratio of the two liquids between $0.1 \leq \lambda_k \leq 10$. Two flow regimes are observed. In the first regime at $0.04 \leq \alpha \leq 0.96$, convective flows appear in both layers and Nu is not sensitive to α. In the second regime at $\alpha \leq 0.02$ or $\alpha \geq 0.98$, convective flow only exists in the thicker layer, while the thinner one is dominated by pure conduction. In this regime, Nu is sensitive to α. To predict Nu in the system in which the two layers are separated by a unique interface, we apply the Grossmann–Lohse theory for both individual layers and impose heat flux conservation at the interface. Without introducing any free parameter, the predictions for Nu and for the temperature at the interface agree well with our numerical results and previous experimental data.

Key words: Bénard convection, multiphase flow, turbulence simulation

† Email addresses for correspondence: klchong@shu.edu.cn, d.lohse@utwente.nl

1. Introduction

Turbulent flows with two layers are ubiquitous in nature and technology: for example, the coupled flows between the ocean and the atmosphere (Neelin, Latif & Jin 1994), the convection of the Earth's upper and lower mantles (Tackley 2000), oil slicks on the sea (Fay 1969) and even cooking soup in daily life. Compared with flow with only a single layer, multilayer flow has more complicated flow dynamics and thus more complicated global transport properties. These are determined by the viscous and thermal coupling between the fluid layers. In order to investigate the heat transport in two-layer thermal turbulence, we choose turbulent Rayleigh–Bénard (RB) convection as our canonical model system. The main question to answer is: How does the global heat transport depend on the ratios of the fluid properties and the thicknesses of the two layers?

Rayleigh–Bénard convection, where a fluid is heated from below and cooled from above, is the most paradigmatic example in the study of global heat transport in turbulent flow (see the reviews of Ahlers, Grossmann & Lohse (2009), Lohse & Xia (2010), Chillà & Schumacher (2012) and Shishkina (2021)). Also, previous studies on multiphase flow have taken RB convection as their model system; for example, the studies on boiling convection (Zhong, Funfschilling & Ahlers 2009; Lakkaraju *et al.* 2013; Wang, Mathai & Sun 2019), ice melting in a turbulent environment (Wang *et al.* 2021) or convection laden with droplets (Pelusi *et al.* 2021; Liu *et al.* 2022). These are mainly dispersed multiphase flow. Here we focus on two-layer RB convection, which is highly relevant in geophysics and industrial applications.

Most studies on two-layer RB convection have hitherto been conducted in the non-turbulent regime (Nataf, Moreno & Cardin 1988; Prakash & Koster 1994; Busse & Petry 2009; Diwakar *et al.* 2014), while only a few studies focused on the turbulent one: Davaille (1999) experimentally studied RB convection with two miscible layers and displayed the temperature profiles in each layer and the deformation of the interface. Experiments of RB convection with two immiscible fluid layers were reported by Xie & Xia (2013), who quantified the viscous and thermal coupling between the layers and showed that the global heat flux weakly depends on the type of coupling, i.e. the heat flux at viscous coupling normalized by that at thermal coupling varies from 0.997 to 1.004.

Next to the experiments, the numerical study by Yoshida & Hamano (2016) focused on the heat transport efficiency in two-layer mantle convection with large viscosity contrasts. Our prior numerical simulations (Liu *et al.* 2021*a*) explored a wide range of Weber numbers and density ratios between the two fluids and revealed the interface breakup criteria in two-layer RB convection. Also, most previous studies have focused on the flow dynamics and behaviour of the interface between the two layers. The issue of global heat transport is still quite unexplored, especially in the turbulent regime.

In the present work, we numerically investigate RB convection through two immiscible fluid layers by two-dimensional (2-D) and three-dimensional (3-D) direct numerical simulations. We first calculate the global heat transport for various layer thicknesses and fluid properties. In addition, we extend the Grossmann–Lohse (GL) theory for standard RB convection to the two-layer system and are able to predict the heat transport of the system. The GL theory (Grossmann & Lohse 2000, 2001, 2002; Stevens *et al.* 2013) is a unifying theory for the effective scaling in thermal convection, which successfully describes how the Nusselt number Nu and the Reynolds number Re depend on the Rayleigh number Ra and the Prandtl number Pr. This theory has been well validated over a wide parameter range by many single-phase experimental and numerical results (Stevens *et al.* 2013). We show that the predictions from the GL theory can be extended to two-layer systems without introducing any new free parameter, and the extended theory agrees well with our

numerical results and with previous experimental data (Wang *et al.* 2019). The GL theory also successfully gives the mean temperature at the interface between the two layers.

The organization of this paper is as follows. The numerical method and set-up are introduced in § 2. The main results are presented in §§ 3–5; namely the flow structure and heat transfer in the two-layer RB convection in § 3, the temperature at the interface in § 4 and the effects of the interface deformability on the heat transfer in § 5. The paper ends with conclusions and an outlook.

2. Numerical method and set-up

In this study, 2-D and 3-D simulations are performed. We consider two immiscible fluid layers (fluid 2 over fluid 1) placed in a domain of dimensions $2H \times 2H \times H$ in three dimensions and $2H \times H$ in two dimensions, with H being the domain height. The numerical method (Liu *et al.* 2021*b*) used here combines the phase-field method (Jacqmin 1999; Ding, Spelt & Shu 2007; Liu & Ding 2015) and a direct numerical simulation solver for the Navier–Stokes equations (Verzicco & Orlandi 1996; van der Poel *et al.* 2015), namely AFiD. This method has been well validated in our previous study (Liu *et al.* 2021*b*).

In the phase field method, which is widely used in multiphase simulations of laminar (Chen *et al.* 2020; Li, Liu & Ding 2020) and turbulent flows (Roccon, Zonta & Soldati 2019, 2021), the interface is represented by contours of the volume fraction C of fluid 1. The corresponding volume fraction of fluid 2 is $1 - C$. The evolution of C is governed by the Cahn–Hilliard equation,

$$\frac{\partial C}{\partial t} + \boldsymbol{\nabla} \cdot (\boldsymbol{u}C) = \frac{1}{Pe}\nabla^2\psi, \tag{2.1}$$

where $\boldsymbol{u}$ is the flow velocity and $\psi = C^3 - 1.5C^2 + 0.5C - Cn^2\nabla^2 C$ the chemical potential. We set the Péclet number $Pe = 0.9/Cn$ and the Cahn number $Cn = 0.75h/H$, where h is the mesh size. We take Pe and Cn according to the criteria proposed in Ding *et al.* (2007), Yue, Zhou & Feng (2010) and Liu & Ding (2015), which approaches the sharp-interface limit and leads to well-converged results with mesh refinement. More numerical details, validation cases and convergence tests can be found in Liu *et al.* (2021*b*).

The flow is governed by the Navier–Stokes equation, the heat transfer equation and the incompressibility condition,

$$\tilde{\rho}\left(\frac{\partial \boldsymbol{u}}{\partial t} + \boldsymbol{u}\cdot\boldsymbol{\nabla}\boldsymbol{u}\right) = -\boldsymbol{\nabla}P + \sqrt{\frac{Pr}{Ra}}\boldsymbol{\nabla}\cdot\left[\tilde{\mu}(\boldsymbol{\nabla}\boldsymbol{u} + \boldsymbol{\nabla}\boldsymbol{u}^T)\right] + \boldsymbol{F}_{st} + \boldsymbol{G}, \tag{2.2}$$

$$\tilde{\rho}\tilde{c_p}\left(\frac{\partial \theta}{\partial t} + \boldsymbol{u}\cdot\boldsymbol{\nabla}\theta\right) = \sqrt{\frac{1}{PrRa}}\boldsymbol{\nabla}\cdot(\tilde{k}\boldsymbol{\nabla}\theta), \tag{2.3}$$

$$\boldsymbol{\nabla}\cdot\boldsymbol{u} = 0, \tag{2.4}$$

respectively, where θ is the dimensionless temperature, $\boldsymbol{F}_{st} = 6\sqrt{2}\psi\boldsymbol{\nabla}C/(CnWe)$ the dimensionless surface tension force and $\boldsymbol{G} = \{[C + \lambda_\beta\lambda_\rho(1 - C)]\,\theta - \tilde{\rho}/Fr\}\boldsymbol{z}$ the dimensionless gravity. All dimensionless fluid properties (indicated by $\tilde{q}$) are defined in a uniform way,

$$\tilde{q} = C + \lambda_q(1 - C), \tag{2.5}$$

where $\lambda_q = q_2/q_1$ is the ratio of the material properties of fluid 2 and fluid 1, marked by the subscripts 2 and 1, respectively. The global dimensionless parameters controlling the flow are: the Rayleigh number (the dimensionless temperature difference between the plates) $Ra = \beta_1 g H^3 \Delta/(\nu_1 \kappa_1)$; the Prandtl number $Pr = \nu_1/\kappa_1$ as ratio between kinematic viscosity and thermal diffusivity; the Weber number (the ratio of inertia to surface tension) $We = \rho_1 U^2 H/\sigma$; and the Froude number (the ratio of inertia to gravity) $Fr = U^2/(gH)$. Here, β is the thermal expansion coefficient, g the gravitational acceleration, Δ the temperature difference between the hot bottom and cold top plate, $\nu = \mu/\rho$ the kinematic viscosity, ρ the density, μ the dynamic viscosity, $\kappa = k/(\rho c_p)$ the thermal diffusivity, k the thermal conductivity, c_p the specific heat capacity, $U = \sqrt{\beta_1 g H \Delta}$ the free-fall velocity and σ the surface tension of the interface between the two fluids. The heat transfer of the system is characterized by the Nusselt number $Nu = Q/(k_1 \Delta/H)$, with Q being the heat flux.

In this study, we investigate how the heat transfer is influenced by the relative layer thickness α (for the upper layer) and the thermal conductivity coefficient ratio λ_k of the upper layer over the lower layer. We vary α from 0 (pure fluid 1) to 1 (pure fluid 2), and $0.1 \leq \lambda_k \leq 10$, which is in an experimentally accessible range, e.g. $\lambda_k \approx 10$ in the experiments by Xie & Xia (2013) and $\lambda_k \approx 8$ in Wang *et al.* (2019). For numerical simplicity, we fix the global parameters: $Ra = 10^8$, at which there is already considerable turbulent intensity; $Pr = 4.38$, based on the property of water; and $We = 5$, a value ensuring that the surface tension is still strong enough so that the interface does not break up. The second term $-\tilde{\rho}/Fr$ of the dimensionless gravity $\boldsymbol{G}$ in (2.2) only determines which fluid is in the lower layer; it has no effect on the flow in each individual layer due to the Boussinesq approximation. We take $Fr = 1$ for numerical convenience. The density ratio $\lambda_\rho = 0.8$, reflecting that fluid 2 in the upper layer is less dense than fluid 1 in the lower layer. For simplicity, the other material properties are the same in both fluids, including β, ν and κ, in order to exclude their effects on the values of Ra and Pr in each layer.

We set the boundary conditions on the plates as $\partial C/\partial z = 0$, no-slip velocities, and fixed temperature $\theta = 0$ (top) and 1 (bottom), and use periodic conditions in the horizontal directions. At the interface, we have the continuity condition of both the velocity and shear stresses. Uniform grids with $1152 \times 1152 \times 576$ gridpoints in the 3-D cases and 1152×576 gridpoints in the 2-D cases are used for the velocity and temperature fields, and $4608 \times 4608 \times 2304$ gridpoints in the 3-D cases and 4608×2304 gridpoints in the 2-D cases for the phase field. Eight gridpoints in the mesh for the phase field are used to describe the diffusive interface. The coupling technique between the two meshes follows Ding & Yuan (2014). For all cases, there are between 5.1 and 6.5 gridpoints to resolve the Kolmogorov scale, and between 9 and 23 gridpoints for the thermal boundary layer and even more for the viscous boundary layer due to $\mathrm{Pr} > 1$, which are sufficiently fine based on Shishkina *et al.* (2010) (less than eight gridpoints are required for the values of Nu, Ra, and Pr at hand here). The reason we use more gridpoints for the Kolmogorov scale than others (normally $1 \sim 2$ gridpoints) is that we are using a uniform mesh, so that the mesh must be sufficiently fine to ensure that there are enough gridpoints in the boundary layers. The mesh is sufficiently fine and is comparable to corresponding single-phase studies in two dimensions and three dimensions (Stevens, Verzicco & Lohse 2010; van der Poel, Stevens & Lohse 2013; Zhang, Zhou & Sun 2017). We take 1000 free-fall time units to obtain sufficient statistics in the 2-D cases, and 250 free-fall time units in the 3-D cases.

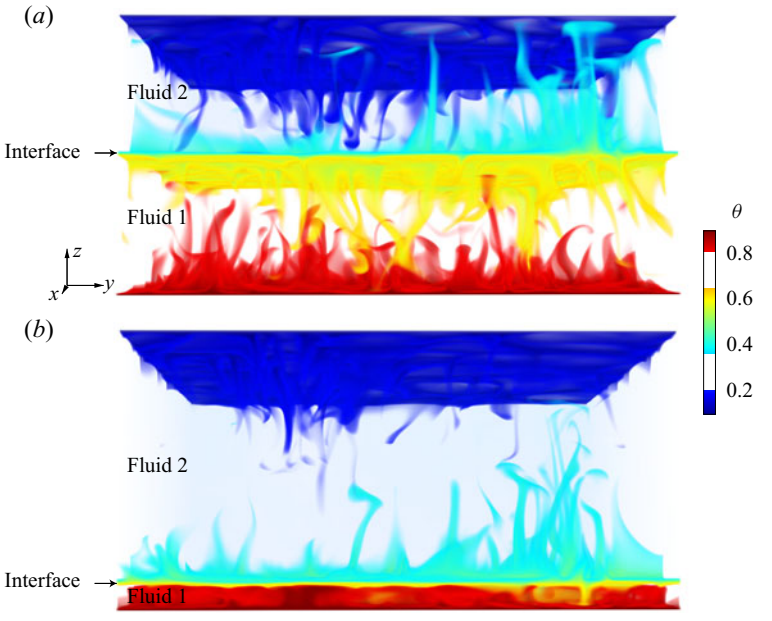

Figure 1. Volume rendering of a snapshot of the thermal structures in two-layer RB convection in 3-D simulations at $Ra = 10^8$, $We = 5$, the thermal conductivity coefficient ratio $\lambda_k = 1$ and the thickness of the upper layer (*a*) $\alpha = 0.5$ and (*b*) $\alpha = 0.9$. The temperature field is colour-coded.

3. Flow structure and heat transfer in the two-layer system

We first examine the typical flow structure in turbulent RB convection with two immiscible fluid layers. Since the Weber number is sufficiently small ($We = 5$), strong enough surface tension prevents the fluid interface from producing droplets, and a clear single interface can be distinguished.

As shown in figure 1 for two 3-D cases and figure 2(*a*,*b*) for three 2-D cases, a large-scale circulation exists in each individual layer, which is consistent with previous two-layer studies (Davaille 1999; Xie & Xia 2013; Liu *et al.* 2021*a*). From figure 2, we also observe that the temperature profile in each layer resembles that in the single-phase flow, namely the temperature remains constant in the bulk of each layer and strongly varies in the boundary layers near the plates and the interface.

When one layer becomes thin enough, we observe a temperature inversion therein (see figure 2*b*). A similar feature has been observed in Blass *et al.* (2021), who considered sheared thermal convection, and in many prior papers (Belmonte, Tilgner & Libchaber 1993; Tilgner, Belmonte & Libchaber 1993; Ahlers *et al.* 2009). The reason for the inversion is that the fluctuations in the flow are not strong enough to fully mix the bulk. Then the remaining hot (cold) fluid is carried downward (upward) by the flow.

When one layer is sufficiently thin, pure thermal conduction instead of convection is observed. This is the case once the local Ra (defined with the layer thickness and its material parameters) becomes smaller than the onset value of convection. For example, in figure 2(*c*), the bottom layer has the local Rayleigh number $Ra_1 = 34.4$ and a pure conductive layer is found. Thus two regimes are identified: the regime with both convective layers appears at $0.04 \leq \alpha \leq 0.96$; and the regime with one conductive layer and one convective layer at $\alpha \leq 0.02$ or $\alpha \geq 0.98$. Since from figures 3(*a*), 4(*b*) and 4(*c*) we observe that heat flux Nu and the interface temperature θ_i in the case of $\alpha = 0.02$ and of $\alpha = 0.04$

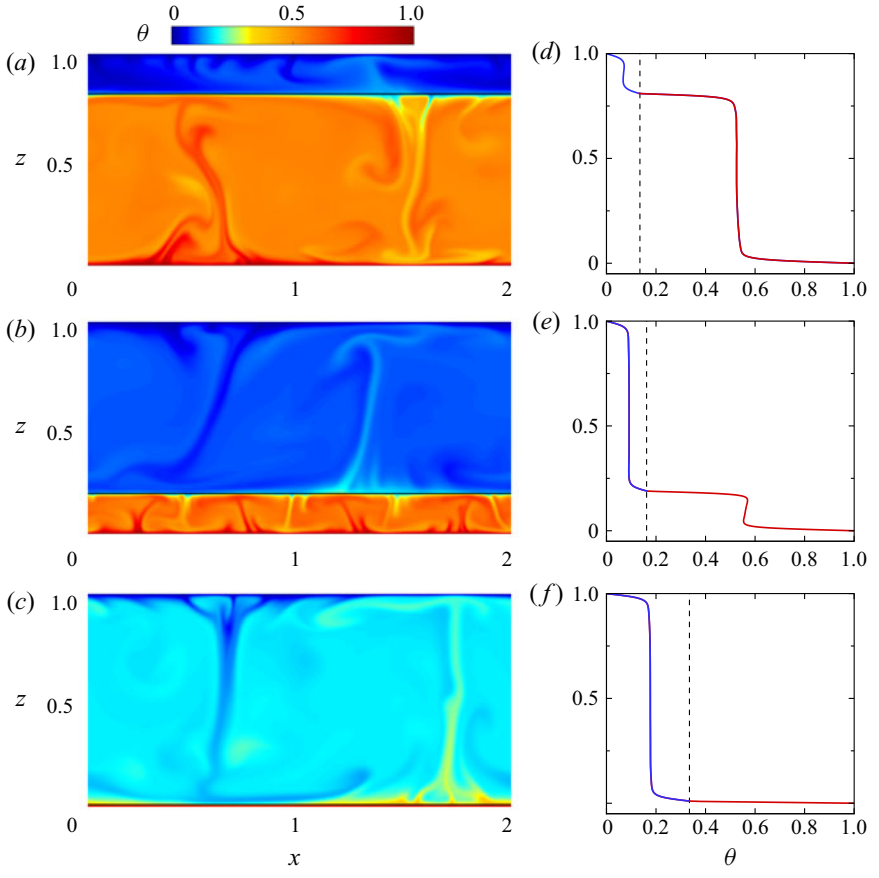

Figure 2. Snapshots of the 2-D simulations at $\lambda_k = 10$ and (*a*) $\alpha = 0.19$, (*b*) $\alpha = 0.81$ and (*c*) $\alpha = 0.99$. The corresponding average (in time and space) temperature profiles are shown as blue (upper layer) and red (bottom layer) curves on panels (*d–f*), where the dashed lines denote the temperature at the interface.

are very similar (the same for $\alpha = 0.96$ and $\alpha = 0.98$), we did not perform more cases in these transition zones of $0.02 < \alpha < 0.04$ and $0.96 < \alpha < 0.98$.

In the two distinct regimes, the heat transfer shows different α dependence as shown in figure 3(*a*), where the heat flux is normalized with the heat flux Nu_s for the single-phase flow (pure fluid 1). In the regime with both convective layers, the heat transfer hardly varies with α although the layer thickness α changes considerably. More specifically, we obtain $0.48 \leq Nu/Nu_s \leq 0.57$ over $0.04 \leq \alpha \leq 0.96$ for $\lambda_k = 1$ while $1.00 \leq Nu/Nu_s \leq 1.59$ for $\lambda_k = 10$. In contrast, in the regime with one conductive layer, with α only increasing from 0.98 to 1, Nu/Nu_s increases largely from 0.72 to 1.00 for $\lambda_k = 1$ and from 1.72 to 10.00 for $\lambda_k = 10$. Note that this interesting dependence of Nu/Nu_s on α also holds for the 3-D cases.

Also the λ_k dependence is examined and shown in figure 3(*b*). As expected, the heat transfer in the two-layer system is limited by the layer with the lower thermal conductivity coefficient.

Obviously, in two-layer RB convection, Nu is affected by more parameters (namely α and the various ratios between the material properties such as λ_k) as compared with the single-phase case. To predict Nu in the two-layer system, we regard the convection in each

layer as single-phase convection. Then we apply the GL theory (Grossmann & Lohse 2000, 2001, 2002; Stevens *et al.* 2013) in each individual layer,

$$(Nu_j - 1)Ra_j Pr_j^{-2} = c_1 \frac{Re_j^2}{g(\sqrt{Re_c/Re_j})} + c_2 Re_j^3, \tag{3.1}$$

$$Nu_j - 1 = c_3 Re_j^{1/2} Pr_j^{1/2} \left\{ f\left[\frac{2aNu_j}{\sqrt{Re_c}} g\left(\sqrt{\frac{Re_c}{Re_j}} \right) \right] \right\}^{1/2} + c_4 Pr_j Re_j f\left[\frac{2aNu_j}{\sqrt{Re_c}} g\left(\sqrt{\frac{Re_c}{Re_j}} \right) \right], \tag{3.2}$$

for $j = 1$ and 2, indicating fluid 1 and 2, respectively. Here the local Rayleigh numbers in the respective layers are $Ra_1 = (1-\alpha)^3(1-\theta_i)Ra$ and $Ra_2 = \alpha^3\theta_i Ra$ with θ_i being the temperature at the interface, and the local Prandtl numbers are $Pr_1 = \nu_1/\kappa_1$ and $Pr_2 = \nu_2/\kappa_2$. Here f and g are crossover functions, which are given by Grossmann & Lohse (2000, 2001). We take the values of the parameters of the theory as given by Stevens *et al.* (2013), namely $c_1 = 8.05$, $c_2 = 1.38$, $c_3 = 0.487$, $c_4 = 0.0252$ and $Re_c = (2c_0)^2$ with $c_0 = 0.922$. These are based on various numerical and experimental data over a large range of Ra and Pr numbers. The above equations can be closed by imposing the heat flux balance at the interface,

$$Q_2 = Q_1. \tag{3.3}$$

These heat fluxes are differently non-dimensionalized as Nusselt numbers, namely

$$\left.\begin{aligned} Nu_2 &= \frac{Q_2}{k_2 \dfrac{\theta_i \Delta}{\alpha H}}, \\ Nu_1 &= \frac{Q_1}{k_1 \dfrac{(1-\theta_i)\Delta}{(1-\alpha)H}}. \end{aligned}\right\} \tag{3.4}$$

With (3.1)–(3.4) we obtain the GL-predictions for $Nu(Ra, Pr)$ for the system with two convective layers.

Just as in single layer RB, the regime with one conductive layer has to be treated differently, instead of simply using (3.1) and (3.2). First, to determine the criteria for the occurrence, we use (3.1)–(3.4) to calculate Ra_1 and Ra_2, and then compare them with the onset value of convection. Note that the conductive layer only occurs when the layer is thin enough, and in that case the aspect ratio of the conductive layer is much larger than 1, allowing us to take the onset value to be 1708 (Chandrasekhar 1981). Next, if one of the local Rayleigh numbers is smaller than 1708, we use $Nu_j = 1$ to replace (3.1) and (3.2). We get the critical layer thickness $\alpha_c = 0.965$ for $\lambda_k = 1$ ($\alpha_c = 0.972$ for $\lambda_k = 10$) at $Ra_1 = 1708$ and $\alpha_c = 0.035$ for $\lambda_k = 1$ ($\alpha_c = 0.057$ for $\lambda_k = 10$) at $Ra_2 = 1708$, which agree well with our simulations.

In figure 3, we compare Nu/Nu_s from the simulations with the predictions above. In both regimes, the dependence of Nu/Nu_s on α and λ_k agrees well with the predictions of the GL theory for the two-layer system. Note that no new fitting parameter was introduced at all.

The strong increase of the heat transfer for $\alpha \leq 0.02$ or $\alpha \geq 0.98$ can qualitatively be understood from the number of the conductive layers in the system. For $\alpha \leq 0.02$ or

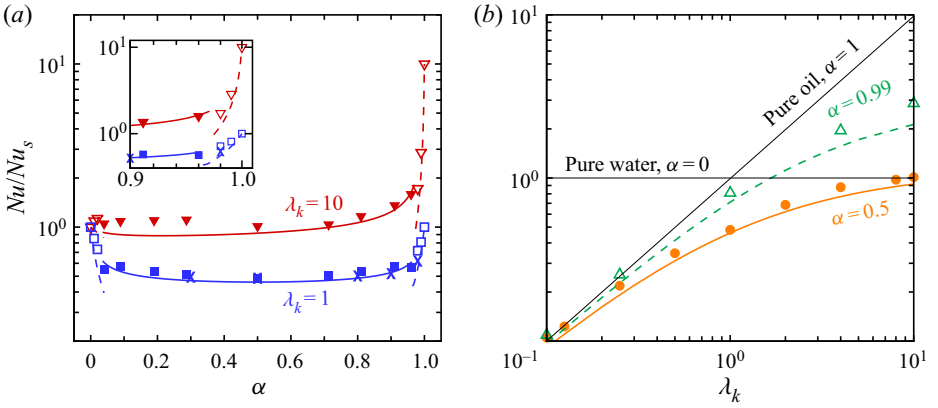

Figure 3. Global Nusselt number Nu normalized by Nu_s of the single-phase system (pure fluid 1) as a function of (*a*) α and (*b*) λ_k at $Ra = 10^8$ and $We = 5$. The symbols denote the numerical results and the lines the GL theory for two-layer system (3.1)–(3.4) at fixed (*a*) $\lambda_k = 1$ and 10 and (*b*) $\alpha = 0.5$ and 0.99, where the filled symbols/solid lines denote the regime with both convective layers, and the empty symbols/dashed lines the regime with one convective layer and one conductive layer. The 3-D cases are marked as cross symbols. The inset in (*a*) shows a zoom-in view for α close to 1.

$\alpha \geq 0.98$ there are only two conductive layers, namely at the top plate and at the bottom plate, and only one convective layer, which provides a thermal shortcut. In contrast, for $0.04 \leq \alpha \leq 0.96$ there are two convective layers (with thermal shortcuts), but three conductive layers (namely, an addition one in between the two convective layers), and all three provide considerable thermal resistance, making the two layer system with two convective layers less heat conductive.

To further validate our quantitative predictions of the extended GL theory, we also compare the theoretical prediction with previous pioneering experiments by Wang *et al.* (2019). These authors successfully created a closed system with highly efficient heat transfer enhancement by adding a minute concentration of heavy oil (HFE-7000) to RB convection of water. Via precise experimental measurements, two regimes could be identified: one is the boiling regime, where a significant heat transfer enhancement is observed and physically explained; and the other one is the non-boiling regime, which is a typical two-layer RB convection. The two layers are a water layer on the top and a heavy oil (HFE-7000) layer at the bottom. Based on the experiment settings of the pioneering work of Wang *et al.* (2019), the parameters chosen here are $Ra \approx 4.5 \times 10^{10}$ and $Pr \approx 8.8$ (calculated for pure water) and $\lambda_\beta \approx 0.044$, $\lambda_\nu \approx 3.8$, $\lambda_\kappa \approx 3.3$ and $\lambda_k \approx 7.7$ (water over oil). In the system with 99 % water and 1 % oil in volume, Wang *et al.* (2019) measured $Nu \approx 102$ (from figure 3*e* of that paper). With the extended GL theory for the two layers (3.1)–(3.4), we obtain a heat transfer $Nu = 90.4$, which reasonably agrees with the experimental results.

4. Temperature at the interface

The mean temperature θ_i (averaged in time and space) of the interface (the contour of $C = 0.5$) plays a crucial role in the heat transfer of the two-layer system, since it determines the value of the local Rayleigh numbers as mentioned in § 3. We plot the α dependence of θ_i in figure 4. Similarly to the α dependence of Nu/Nu_s, we again observe that θ_i is

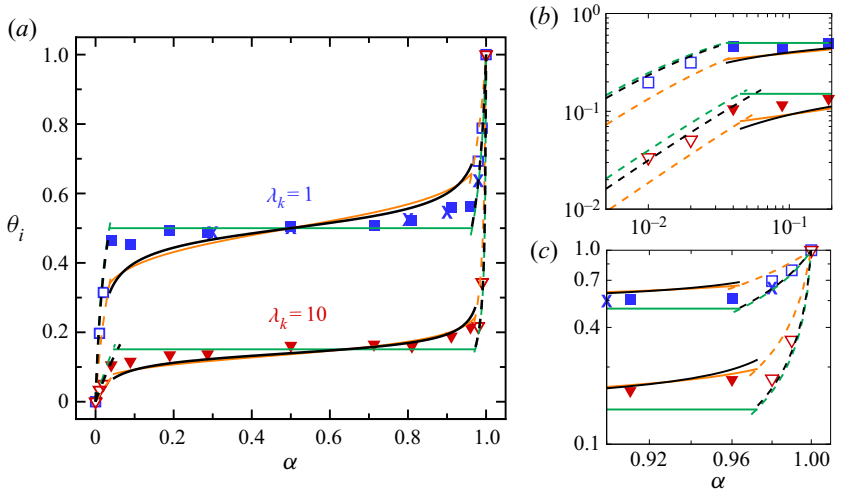

Figure 4. Temperature at the interface θ_i as function of α. Panels (b,c) are zoom-in views of (a). The lines represent the GL theory for the two-layer system (black) in (3.1)–(3.4), and the approximate theory in (4.1)–(4.6) with Nu versus Ra scaling exponent of $\gamma = 1/4$ (orange) and $\gamma = 1/3$ (green). The symbols and line types are the same as in figure 3. The temperature distribution is not uniform on the interface. The error bar (i.e. the standard deviation of the temperature) for each case is smaller than the symbol size.

insensitive to the change in α over $0.04 \leq \alpha \leq 0.96$, whereas significant changes in θ_i are observed for $\alpha \leq 0.02$ or $\alpha \geq 0.98$.

To explain this α dependence of the mean temperature θ_i of the interface, we again use the GL theory to estimate $Nu(Ra, Pr)$ in each of the two layers and then plug the results into (3.4) to obtain $\theta_i(\alpha, \lambda_k)$. The results are shown as black lines in figure 4 (for the $\theta_i(\alpha)$ dependence) and figure 5 (for the $\theta_i(\lambda_k)$ dependence), where the GL-predictions for the interfacial temperature $\theta_i(\alpha, \lambda_k)$ agree very well with the numerical results, demonstrating once more the predictive power of the GL theory.

The strong decrease (increase) of the interfacial temperature θ_i for small $\alpha \leq 0.02$ (large $\alpha \geq 0.98$) in figure 4 can straightforwardly be understood by the proximity of the interface to the cold (hot) plate and our above explanations of the α-dependence of Nu. The λ_k-dependence of θ_i in figure 5 can qualitatively be understood as follows. To ensure the heat flux conservation at the interface, for large $\lambda_k > 1$ (namely, larger thermal conductivity of the fluid in the top layer than in the bottom one) the temperature difference between the interface and the cold top plate ($\theta_i - 0$) must be smaller. This argument also implies a decrease of the interfacial temperature θ_i with increasing λ_k.

For the above-mentioned case of Wang *et al.* (2019) for the water–heavy-oil two-layer RB convection, our theory gives a mean interface temperature $\theta_i = 0.53$, i.e. slightly enhanced as compared with the case $\theta_i = 1/2$, which would occur if the material properties of the two layers were identical. This slight increase reflects that $\kappa_1 < \kappa_2$, and that consequently the bottom thermal BL is thinner than the top one, leading to a better thermal coupling of the centre interface to the hot bottom plate as compared with the cold top one, similarly as in non-Oberbeck–Boussinesq thermal convection with water (Ahlers *et al.* 2006), where the hot bottom thermal BL is also thinner than the cold top one and the mean bulk temperature enhanced. Note that in their experiments, Wang *et al.* (2019) could not provide experimental data for the interface temperature, as this would experimentally be too challenging; so here we cannot compare with experiment.

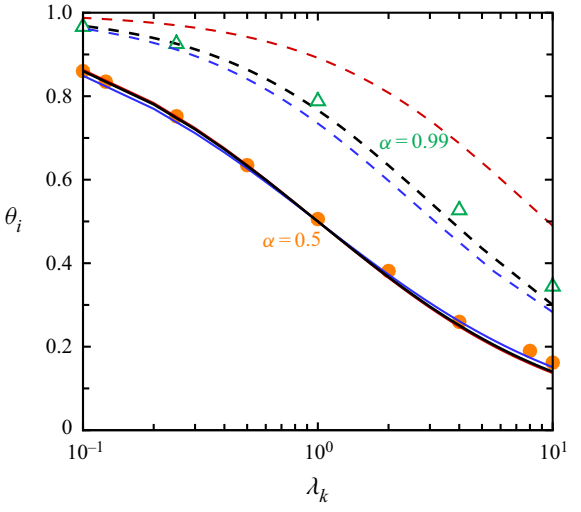

Figure 5. Temperature at the interface θ_i as function of λ_k. The lines represent the full GL theory for the two-layer system (black) in (3.1)–(3.4) and the approximate theory in (4.3) and (4.5) with *Nu* versus *Ra* scaling exponent of $\gamma = 1/4$ (red) and $\gamma = 1/3$ (blue). All the cases here are 2-D cases. The symbols and line types are the same as in figure 3.

To obtain a simple relationship for $\theta_i(\alpha, \lambda_k)$, rather than using the full GL theory, an abbreviated approach is to just use an effective scaling exponent γ to approximate the full GL theory, ignoring the crossovers between the regimes,

$$Nu_j \sim Ra_j^{\gamma}, \tag{4.1}$$

where γ and the prefactor are constant when *Ra* varies over a small range.

Then, by applying (4.1) in each layer and imposing the heat flux balance at the interface (3.3) and (3.4), we obtain

$$[(1-\alpha)^3(1-\theta_i)Ra]^{\gamma} k_1 \frac{(1-\theta_i)\Delta}{(1-\alpha)H} = (\alpha^3\theta_i Ra)^{\gamma} k_2 \frac{\theta_i \Delta}{\alpha H}. \tag{4.2}$$

Note that the prefactor of (4.1) cancels out. After rewriting equation (4.2), we get the following approximate scaling law for the regime with two convective layers:

$$\frac{1}{\theta_i} - 1 = \lambda_k^{1/(1+\gamma)} \left(\frac{1}{\alpha} - 1\right)^{(1-3\gamma)/(1+\gamma)}. \tag{4.3}$$

We now consider the value of γ to vary between $1/4$ and $1/3$, which is reasonable for the classical regime of RB convection (Ahlers *et al.* 2009; Lohse & Xia 2010; Chillà & Schumacher 2012; Shishkina 2021). Correspondingly, the exponent $(1-3\gamma)/(1+\gamma)$ in (4.3) varies from 0.2 to 0. This low value reflects the relatively weak α dependence of θ_i for the regime with two convective layers.

To validate the simplified relationship (4.3), we show the results for $\gamma = 1/4$ and $1/3$ in figure 4(*a*) and figure 5. In both figures, the numerical data and the full GL predictions are in-between the simple relationship of (4.3) with $\gamma = 1/4$ and that one with $\gamma = 1/3$, since a constant effective exponent γ is appropriately only within a small range of *Ra* while the full GL theory well describes a wide range of *Ra*.

For the cases with the lower layer being thin enough to be purely conductive (i.e. $\alpha \to 1$), we must use $Nu_1 = 1$ in the lower layer together with (4.1) for the upper layer, which gives

$$k_1 \frac{(1-\theta_i)\Delta}{(1-\alpha)H} \sim (\alpha^3 \theta_i Ra)^\gamma k_2 \frac{\theta_i \Delta}{\alpha H}. \tag{4.4}$$

Then, by rewriting this equation, we obtain

$$\frac{1-\theta_i}{\theta_i^{(1+\gamma)}} \sim \lambda_k \, \alpha^{3\gamma-1}(1-\alpha). \tag{4.5}$$

Although the term $\alpha^{3\gamma-1}$ has only weak α dependence (considering γ to be between $1/4$ and $1/3$), θ_i is sensitive to α because of the term $1-\alpha$. We obtain the prefactor in (4.5) by matching (4.5) and (4.3) at $Ra_1 = 1708$, since (4.5) is applicable for $Ra_1 \leq 1708$ and (4.3) for $Ra_1 \geq 1708$.

Similarly, in the case when the upper layer is purely conductive ($\alpha \to 0$), we obtain

$$\frac{\theta_i}{(1-\theta_i)^{1+\gamma}} \sim \lambda_k \, (1-\alpha)^{3\gamma-1}\alpha, \tag{4.6}$$

which also indicates that θ_i is sensitive to α in that regime. Furthermore, (4.3)–(4.6) show that θ_i is sensitive to λ_k in all the situations.

Also for these regimes with $\alpha \leq 0.02$ or $\alpha \geq 0.98$ we validate the derived approximate relations (4.5) and (4.6) using $\gamma = 1/4$ and $\gamma = 1/3$ in figures 4(*b*), 4(*c*) and 5. Again, good agreements are achieved also in these regimes with one conductive layer and one convective layer.

5. Effects of the deformable interface

In RB convection with two layers, the large-scale circulations are confined within each layer provided that the surface tension is strong enough, i.e. *We* small enough. For example, for $We = 5$ as in our simulations, the interface only deforms slightly as can be seen in figures 1 and 2. However, on increasing *We*, the interface becomes wavy (see figure 6*a*) and even breaks up (see figure 6*b*). We have derived the criterion for interface breakup in our previous study (Liu *et al.* 2021*a*).

In the wavy case, the large-scale circulation still exists in each layer. In contrast, in the breakup case, the surface tension is too weak and stirring of the fluid layers takes place as evidenced by the vanishing of the sharp temperature jump in the middle of the cell in figure 6(*c*).

The Nusselt number also exhibits a highly non-trivial *We* dependence, in accordance with the quite different flow dynamics. When the interface remains intact, the values of Nu/Nu_s are close to the prediction from the extended GL theory for the two-layer system. When there is a wavy interface, Nu/Nu_s becomes slightly larger than the GL prediction. However, when the interface breaks up, Nu/Nu_s directly jumps to a saturated value, which is slightly smaller than the value obtained for single-phase flow of the better conducting layer. The reason for the slight difference to the single phase RB case is that although a clear two-layer structure has been washed out, the existence of the heavy droplets of fluid 1 and the light ones of fluid 2 will anyhow slow down the convective flow, hindering the heat flux.

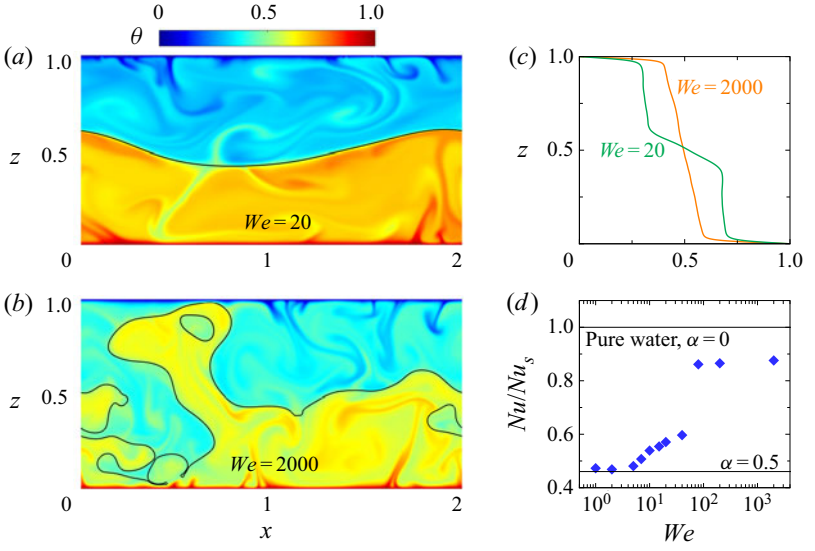

Figure 6. (*a*) Snapshots with the wavy interface at $We = 20$ and (*b*) with the breakup interface at $We = 2000$. (*c*) Corresponding average temperature profiles. (*d*) Here Nu/Nu_s as a function of We. The lines represent the extended GL theory for the two-layer system, ignoring the interface dynamics. All the cases here are 2-D cases at fixed $Ra = 10^8$, $\alpha = 0.5$ and $\lambda_k = 1$.

6. Conclusions and outlook

Turbulent RB convection with two immiscible fluid layers is numerically investigated for various layer thicknesses ($0.01 \leq \alpha \leq 0.99$) and thermal conductivity coefficient ratios ($1 \leq \lambda_k \leq 10$) both in two dimensions and three dimensions. Two regimes can be identified: in regime 1, two convective layers appear; while in regime 2, one layer is sufficiently thin and dominated by pure conduction because the local Ra thereof is smaller than the onset value of convection. The heat transfer Nu is sensitive to the layer thickness α in regime 2 but not in regime 1. To explain the observed Nu behaviours, we extend the GL theory of single-phase RB convection to the two-layer system. The predictions from the extended GL theory for the overall heat transport agree well with the simulations for various λ_k and also with experimental data. Moreover, the temperature at the interface can also be predicted nicely for the two-layer system. We further derived a simple scaling model to explicitly show the relationship between θ_i, α and λ_k. Finally, the effect of the deformable interface on the heat transfer is studied, where we find that the extended GL theory for the two-layer system still roughly holds, as long as the interface does not break up.

This study showed that the extended GL theory for the two-layer system works for various ratios of the thermal conductivity coefficient in two layers, which is a key property among all material properties, but we expect that the theory also holds when we vary the ratio of other properties, e.g. the thermal expansion coefficient, the density, the dynamic viscosity, the thermal diffusivity (as had already been done in the pioneering experiment of Wang *et al.* (2019)) and the specific heat capacity. The ratios of all properties can be represented by the local dimensionless numbers Ra_1, Ra_2, Pr_1 and Pr_2 in the extended GL theory. It would be also interesting to test this theory for various other global Ra and Pr, which here were fixed at $Ra = 10^8$ and $Pr = 4.38$.

The results in this work can find many realistic applications, such as in atmospheric oceanography, geophysics and industry. Our main finding, the layer thickness dependence of heat transport in the two-layer system, also suggests that the two-layer system is not a good choice if one wants to enhance the overall heat transfer. When the two-layer system is unavoidable anyhow, to ensure the maximal heat transfer, the layer with the lower thermal conductivity coefficient must be kept thin enough to ensure that pure conduction occurs in this layer, which then is identical to the thermal boundary layer at the corresponding plate. For thicker liquid layers the heat transfer has to overcome three conductive layers, namely the two at the plates and one extra one between the two convective layers, and the thermal resistance is correspondingly larger and the overall heat transfer lower.

Acknowledgments. We acknowledge PRACE for awarding us access to MareNostrum in Spain at the Barcelona Computing Center (BSC) under the project nos. 2020225335 and 2020235589. K.L.C. acknowledges the Shanghai Science and Technology Program under project no. 19JC1412802. This work was also carried out on NWO Domain Science for the use of the national computer facilities.

Funding. The work was financially supported by an ERC-Advanced Grant under the project no. 740479 and the NWO Max Planck Centre 'Complex Fluid Dynamics'.

Declaration of interests. The authors report no conflict of interest.

Author ORCIDs.
Hao-Ran Liu https://orcid.org/0000-0001-7754-9454;
Kai Leong Chong https://orcid.org/0000-0002-3182-3689;
Rui Yang https://orcid.org/0000-0002-9870-6743;
Roberto Verzicco https://orcid.org/0000-0002-2690-9998;
Detlef Lohse https://orcid.org/0000-0003-4138-2255.

References

Ahlers, G., Brown, E., Fontenele Araujo, F., Funfschilling, D., Grossmann, S. & Lohse, D. 2006 Non-Oberbeck–Boussinesq effects in strongly turbulent Rayleigh–Bénard convection. *J. Fluid Mech.* **569**, 409–445.

Ahlers, G., Grossmann, S. & Lohse, D. 2009 Heat transfer and large scale dynamics in turbulent Rayleigh–Bénard convection. *Rev. Mod. Phys.* **81**, 503–537.

Belmonte, A., Tilgner, A. & Libchaber, A. 1993 Boundary layer length scales in thermal turbulence. *Phys. Rev. Lett.* **70**, 4067–4070.

Blass, A., Tabak, P., Verzicco, R., Stevens, R.J.A.M. & Lohse, D. 2021 The effect of Prandtl number on turbulent sheared thermal convection. *J. Fluid Mech.* **910**, A37.

Busse, F.H. & Petry, M. 2009 Homologous onset of double layer convection. *Phys. Rev.* E **80**, 046316.

Chandrasekhar, S. 1981 *Hydrodynamic and Hydromagnetic Stability*. Dover.

Chen, H., Liu, H.-R., Gao, P. & Ding, H. 2020 Submersion of impacting spheres at low Bond and Weber numbers owing to a confined pool. *J. Fluid Mech.* **884**, A13.

Chillà, F. & Schumacher, J. 2012 New perspectives in turbulent Rayleigh–Bénard convection. *Eur. Phys. J.* E **35**, 58.

Davaille, A. 1999 Simultaneous generation of hotspots and superswells by convection in a heterogeneous planetary mantle. *Nature* **402**, 756–760.

Ding, H., Spelt, P.D.M. & Shu, C. 2007 Diffuse interface model for incompressible two-phase flows with large density ratios. *J. Comput. Phys.* **226**, 2078–2095.

Ding, H. & Yuan, C. 2014 On the diffuse interface method using a dual-resolution Cartesian grid. *J. Comput. Phys.* **273**, 243–254.

Diwakar, S.V., Tiwari, S., Das, S.K. & Sundararajan, T. 2014 Stability and resonant wave interactions of confined two-layer Rayleigh–Bénard systems. *J. Fluid Mech.* **754**, 415–455.

Fay, J.A. 1969 The spread of oil slicks on a calm sea. In *Oil on the Sea* (ed. D.P. Hoult), pp. 53–63. Cambridge University Press.

Grossmann, S. & Lohse, D. 2000 Scaling in thermal convection: a unifying view. *J. Fluid Mech.* **407**, 27–56.

GROSSMANN, S. & LOHSE, D. 2001 Thermal convection for large Prandtl number. *Phys. Rev. Lett.* **86**, 3316–3319.

GROSSMANN, S. & LOHSE, D. 2002 Prandtl and Rayleigh number dependence of the Reynolds number in turbulent thermal convection. *Phys. Rev.* E **66**, 016305.

JACQMIN, D. 1999 Calculation of two-phase Navier–Stokes flows using phase-field modeling. *J. Comput. Phys.* **155**, 96–127.

LAKKARAJU, R., STEVENS, R.J.A.M., ORESTA, P., VERZICCO, R., LOHSE, D. & PROSPERETTI, A. 2013 Heat transport in bubbling turbulent convection. *Proc. Natl Acad. Sci. USA* **110** (23), 9237–9242.

LI, H., LIU, H.-R. & DING, H. 2020 A fully 3D simulation of fluid-structure interaction with dynamic wetting and contact angle hysteresis. *J. Comput. Phys.* **420**, 109709.

LIU, H.-R., CHONG, K.L., NG, C.S., VERZICCO, R. & LOHSE, D. 2022 Enhancing heat transport in multiphase Rayleigh–Bénard turbulence by changing the plate-liquid contact angles. *J. Fluid Mech.* **933**, R1.

LIU, H.-R., CHONG, K.L., WANG, Q., NG, C.S., VERZICCO, R. & LOHSE, D. 2021*a* Two-layer thermally driven turbulence: mechanisms for interface breakup. *J. Fluid Mech.* **913**, A9.

LIU, H.-R. & DING, H. 2015 A diffuse-interface immersed-boundary method for two-dimensional simulation of flows with moving contact lines on curved substrates. *J. Comput. Phys.* **294**, 484–502.

LIU, H.-R., NG, C.S., CHONG, K.L., VERZICCO, R. & LOHSE, D. 2021*b* An efficient phase-field method for turbulent multiphase flows. *J. Comput. Phys.* **446**, 110659.

LOHSE, D. & XIA, K.-Q. 2010 Small-scale properties of turbulent Rayleigh–Bénard convection. *Annu. Rev. Fluid Mech.* **42**, 335–364.

NATAF, H.C., MORENO, S. & CARDIN, P. 1988 What is responsible for thermal coupling in layered convection? *J. Phys.* **49**, 1707–1714.

NEELIN, J.D., LATIF, M. & JIN, F.F. 1994 Dynamics of coupled ocean-atmosphere models: the tropical problem. *Annu. Rev. Fluid Mech.* **26**, 617–659.

PELUSI, P., SBRAGAGLIA, M., BENZI, R., SCAGLIARINI, A., BERNASCHI, M. & SUCCI, S. 2021 Rayleigh–Bénard convection of a model emulsion: anomalous heat-flux fluctuations and finite-size droplet effects. *Soft Matt.* **17**, 3709–3721.

VAN DER POEL, E.P., OSTILLA-MÓNICO, R., DONNERS, J. & VERZICCO, R. 2015 A pencil distributed finite difference code for strongly turbulent wall-bounded flows. *Comput. Fluids* **116**, 10–16.

VAN DER POEL, E.P., STEVENS, R.J.A.M. & LOHSE, D. 2013 Comparison between two- and three-dimensional Rayleigh–Bénard convection. *J. Fluid Mech.* **736**, 177–194.

PRAKASH, A. & KOSTER, J.N. 1994 Convection in multiple layers of immiscible liquids in a shallow cavity. I. Steady natural convection. *Intl J. Multiphase Flow* **20** (2), 383–396.

ROCCON, A., ZONTA, F. & SOLDATI, A. 2019 Turbulent drag reduction by compliant lubricating layer. *J. Fluid Mech.* **863**, R1.

ROCCON, A., ZONTA, F. & SOLDATI, A. 2021 Energy balance in lubricated drag-reduced turbulent channel flow. *J. Fluid Mech.* **911**, A37.

SHISHKINA, O. 2021 Rayleigh–Bénard convection: the container shape matters. *Phys. Rev. Fluids* **6**, 090502.

SHISHKINA, O., STEVENS, R.J.A.M., GROSSMANN, S. & LOHSE, D. 2010 Boundary layer structure in turbulent thermal convection and its consequences for the required numerical resolution. *New J. Phys.* **12** (7), 075022.

STEVENS, R.J.A.M., VAN DER POEL, E.P., GROSSMANN, S. & LOHSE, D. 2013 The unifying theory of scaling in thermal convection: the updated prefactors. *J. Fluid Mech.* **730**, 295–308.

STEVENS, R.J.A.M., VERZICCO, R. & LOHSE, D. 2010 Radial boundary layer structure and Nusselt number in Rayleigh–Bénard convection. *J. Fluid Mech.* **643**, 495–507.

TACKLEY, P.J. 2000 Mantle convection and plate tectonics: toward an integrated physical and chemical theory. *Science* **288**, 2002–2007.

TILGNER, A., BELMONTE, A. & LIBCHABER, A. 1993 Temperature and velocity profiles of turbulence convection in water. *Phys. Rev.* E **47**, R2253–R2256.

VERZICCO, R. & ORLANDI, P. 1996 A finite-difference scheme for three-dimensional incompressible flow in cylindrical coordinates. *J. Comput. Phys.* **123**, 402–413.

WANG, Z., CALZAVARINI, E., SUN, C. & TOSCHI, F. 2021 How the growth of ice depends on the fluid dynamics underneath. *Proc. Natl Acad. Sci.* **118**, e2012870118.

WANG, Z., MATHAI, V. & SUN, C. 2019 Self-sustained biphasic catalytic turbulence. *Nat. Commun.* **10**, 3333.

XIE, Y.-C. & XIA, K.-Q. 2013 Dynamics and flow coupling in two-layer turbulent thermal convection. *J. Fluid Mech.* **728**, R1.

YOSHIDA, M. & HAMANO, Y. 2016 Numerical studies on the dynamics of two-layer Rayleigh–Bénard convection with an infinite Prandtl number and large viscosity contrasts. *Phys. Fluids* **28**, 116601.

YUE, P., ZHOU, C. & FENG, J.J. 2010 Sharp-interface limit of the Cahn–Hilliard model for moving contact lines. *J. Fluid Mech.* **645**, 279–294.

ZHANG, Y., ZHOU, Q. & SUN, C. 2017 Statistics of kinetic and thermal energy dissipation rates in two-dimensional turbulent Rayleigh–Bénard convection. *J. Fluid Mech.* **814**, 165–184.

ZHONG, J.-Q., FUNFSCHILLING, D. & AHLERS, G. 2009 Enhanced heat transport by turbulent two-phase Rayleigh–Bénard convection. *Phys. Rev. Lett.* **102** (12), 124501.